CuO supported on COK-12 and SBA-15 ordered mesoporous materials for temperature swing SOx adsorption

Julie Schobing, Moisés Cesario, Sophie Dorge, Habiba Nouali, Joël Patarin, Johan Martens, Jean-Francois Brilhac

CuO Supported on COK-12 and SBA-15 Ordered Mesoporous Materials for Temperature Swing SO_x Adsorption

Julie Schobing[1,2,3], Moisés Cesario[1,2,3],Sophie Dorge[1,3], Habiba Nouali[2,3], Joël Patarin[2,3], Johan Martens[4], Jean-François Brilhac[1,3]

[1] Laboratoire de Gestion des Risques et Environnement, Université de Haute Alsace, 3 bis, rue Alfred Werner, 68093 Mulhouse Cedex, France

* Corresponding author: sophie.dorge@uha.fr, phone: +33 3 89 33 61 59, fax: +33 3 89 33 61 61;

julie.schobing@uha.fr; moisesrcesario@gmail.com; jean-francois.brilhac@uha.fr

[2] Equipe Matériaux à Porosité Contrôlée, Institut de Science des Matériaux de Mulhouse, UMR CNRS 7361, Université de Haute-Alsace, 3 bis, rue Alfred Werner, 68093 Mulhouse Cedex, France

habiba.nouali@uha.fr; joel.patarin@uha.fr

[3] Université de Strasbourg, 67000 Strasbourg, France.

[4] University of Leuven, Centre for Surface Chemistry and Catalysis, Celestijnenlaan 200F, B-3001 Heverlee, Belgium

johan.martens@kuleuven.be

Abstract

Ordered mesoporous SBA-15 and COK-12 supports with similar mesopore diameter were loaded with 15 wt.% of CuO and evaluated as adsorbents in a desulfurization process involving SO_x

adsorption and regeneration. Both SBA-15 and COK-12 have a hexagonal arrangement of parallel tubular mesopores. The impact of relatively small differences of the structural and textural properties of the two supports on SO_x adsorption and regenerability is investigated. After impregnation with copper nitrate solution and calcination at 500 ºC, the samples do not show any characteristic XRD pattern of copper-based phases, confirming the highly dispersed state of CuO, which is also checked by Transmission Electron Microscopy (TEM). The COK-CuO15 sample has slightly higher porosity than the SBA-CuO15 sample. The pore volume of both supports is slightly reduced after impregnation-calcination and shaping (Pelletized, Crushed and Sieved – PCS) steps. As for its SOx adsorptive properties, after fifteen adsorption-regeneration cycles at 400 °C, the COK-CuO15_PCS sample exhibits dynamic and total adsorption capacities higher than those of the SBA-CuO15_PCS adsorbent. In addition, both adsorbents preserve their adsorption capacities over the fifteen cycles. The COK-12 support for the CuO active phase provides very promising results in comparison with the literature data for SBA-CuO15 adsorbent.

Keywords: COK-12; SBA-15; CuO-based adsorbents; porosity; SO_x adsorption capacity.

1. Introduction

SO_x is a hazardous by-product of fossil fuel combustion and many industrial processes. The exploitation of thermoelectric power plants and especially those based on coal, petroleum refining, the production of natural gas and the refining of metal ores, are the main sources of SO_x. It is known that the adsorption of sulphur oxides on atmospheric particles, especially from urban or industrial pollution, substantially provokes deleterious effects on human's health (asthmatic diseases, respiratory diseases, etc.). It also impacts the environment (acid rain and formation of atmospheric aerosols) [1-3]. Therefore, the reduction of SO_x gas emissions in

industrial and/or urban areas, especially in heavily populated areas, is highly desirable. The use of regenerable SO_x adsorbents is a very promising approach [1, 4]. It is an alternative to the conventional industrial flue gas desulfurization processes (dry or wet lime injection) currently implemented, which are very energy-intensive and produce little or no recoverable gypsum waste.

SO_x contained in combustion gases are mostly SO_2. SO_x adsorbents should be able to catalyse the oxidation of SO_2 to SO_3 ($SO_2 + ½\ O_2 \rightarrow SO_3$), chemisorb SO_3 as metal sulphates ($x\ SO_3 + MO_x \rightarrow M(SO_4)_x$) and be regenerable by decomposing the sulphate salt ($M(SO_4)_x \rightarrow x\ SO_3 + MO_x$) at relatively low temperature [5].

Several copper-based adsorbent materials have been studied for this purpose [6-9]. CuO has been studied as the active phase due to its good catalytic activity towards SO_2 oxidation and its ability to make sulphate salt by chemisorb SO_3 as $CuSO_4$ [1, 4, 5]. In addition, it can be easily regenerated by simple heat treatment under a reducing atmosphere at a temperature of 400 °C [4]. The use of a support for CuO is essential to improve the dispersion and the reactivity associated with it and the regenerability of the adsorbent subjected to adsorption-regeneration cycles. Alumina-supported copper adsorbents have been reported in the literature, but alumina may react with SO_2 forming species more difficult to decompose which may compromise the performance and lifetime of the adsorbent [6, 9-14]. Activated carbon-supported copper adsorbents have also been investigated, but they have the drawback of retaining some SO_3 by physisorption which complicates the adsorption-desorption process [7, 15-17]. SBA-15 ordered mesoporous silica-supported CuO adsorbents offer quite promising prospects. In fact, these adsorbents combine high adsorption capacities and excellent stability and regenerability in adsorption-desorption cycles at 400 °C [4, 5]. Ordered mesoporous silica like SBA-15 is an attractive support due to its high specific surface in mesopores that allows good dispersion of the active phase [5, 18, 19]. Moreover, its pore diameter (5 -10 nm) ensures good diffusion of

gaseous pollutants towards the active CuO species [5, 18-20]. Ordered mesoporous silica is also chemically inert and thermally stable in the SO_x adsorption process.

However, the synthesis of SBA-15 type materials involves relatively expensive precursors, being carried out under strongly acidic conditions in presence of concentrated HCl. Previous works reported the synthesis of ordered mesoporous silica called COK-12 with mesopore architecture similar to SBA-15 ~~as~~ at quasi-neutral pH, in the presence of citric acid/citrate buffer solution. This method does not use chemically aggressive conditions, can be performed in a continuous process and can be adapted for shaping and forming into tablets, foams and structured catalysts [21-28]. Thus, COK-12 may be considered as an attractive alternative to SBA-15 from a manufacturing point of view. COK-12 has been reported to be an excellent support for many applications, including catalysis on supported metal compounds such as Ni, Pd, TiO_2 and Pt/TiO_2, Na_2WO_4-Mn_xO_y, Co_3O_4, and molybdenum and iron oxides [25, 29-37]. Further applications of COK-12 are the synthesis of mixed matrix membranes [38], fluorescence of dye-loaded COK-12 [39], and drug delivery applications [40]. CuO loaded COK-12 has not been reported before. In this work the application potential of CuO loaded COK-12 in adsorptive separation of SO_x from flue gases, was evaluated and compared to SBA-15-CuO adsorbent.

2. Experimental methods

2.1 Synthesis of SBA-15 and COK-12 ordered mesoporous silica

The SBA-15 ordered mesoporous silica was synthesized as follows: 10.5 g of Pluronic P123 were dissolved in a solution containing 50 mL of HCl (37%) and 330 mL of distilled water in a 500 mL beaker at 55 °C. After complete dissolution, 22.5 g of tetraethylorthosilicate were added and the solution was kept under stirring at 55 °C for 24 h. The temperature was then increased until 90 ºC for 24 h. The precipitate obtained was isolated by centrifugation, washed with

distilled water, dried at 60 ºC overnight and calcined in ceramic plate at 300 ºC for 6 h (ramp of 1 ºC.min^{-1}) in order to remove the organic template.

COK-12 was synthesized as follows. Pluronic P123 (4.05 g), citric acid monohydrate (3.65 g) and trisodium citrate dehydrate (2.62 g) were dissolved in distilled water (107.55 g). The solution was stirred overnight at room temperature. In a separate recipient, sodium waterglass (10.44 g) was diluted with distilled water (30.21 g) and added to the previous mixture at once under stirring. The new mixture was aged for 24 h without stirring at room temperature and then heated at 75 °C for 48 h in a closed recipient. The COK-12 product was recovered by filtering (with polypropylene Millipore filters) and purified by rinsing with distilled water. It was dried at 80 °C. Calcination of the dry material was done in ceramic plate at 550 °C using a heating rate of 1 °C.min^{-1} in order to remove the organic template.

2.2 Preparation of SBA-CuO15 and COK-CuO15 samples

608 g of $Cu(NO_3)_2 \cdot 3H_2O$ was dissolved in 20 mL of distilled water. 3 g of support powder was added to this solution and then stirred at 200 rpm for 4 h at room temperature. The beaker containing the mixture was introduced in a water bath heated at 60 °C, under stirring, until the water was completely evaporated. Afterwards, support powder impregnated with copper nitrate (15 wt.% of CuO) is dried overnight at 60 °C in an oven. Then, the impregnated powder is calcined under synthetic air flow (60 NL.h^{-1}) in a fixed-bed reactor (Ø = 5 cm) at 500 °C for 6 h using a heating rate of 1 °C min^{-1}.

For the SO_2 adsorption experiments, the SBA-CuO15 or COK-CuO15 powders were Pelletized (0.25 t.cm^{-2}, 2 min), Crushed and Sieved using a 250-355 µm sieve (SBA-CuO15_PCS and COK-CuO15_PCS samples, respectively).

Table 1 shows the nomenclature adopted for all samples under investigation.

(Table 1)

120

121 2.3 Characterization of samples

122 Powders were characterized by X-Ray Diffraction (XRD), X-Ray Fluorescence (XRF),
123 Transmission Electron Microscopy (TEM) and N_2 physisorption.

124 X-Ray powder Diffraction was performed in a reflection mode on a PANalytical X'Pert
125 diffractometer (Cu Kα radiation, λ =1.5418 Å) equipped with an X'Celerator detector.
126 Measurements were achieved for 2θ angle values in the 5−70° range, by step of 0.02°, with a
127 time of 220 s by step.

128 The same diffractometer was used to record the XRD patterns at low angles (2θ range from 0.7
129 to 5°). A glass support was used as sample holder that was attached directly to the apparatus.
130 Under these conditions, the thickness of the deposited powder can vary from one sample to the
131 others. Therefore, a variation of peaks' intensity, but also a shift along 2θ axis of the XRD
132 pattern, can be observed. Consequently, it is difficult to give an uncertainty of the unit cell
133 parameter a_{hex}.

134 The copper oxide content in the samples was determined by X-Ray Fluorescence spectrometer
135 (Philips MagiX) on samples previously compacted in 13 mm diameter pellets. From numerous
136 experiences realised on standard materials, the relative uncertainty of copper content is equal to
137 2%. In this case, the uncertainty of the measurement has been estimated from the appropriate
138 Student's t (to obtain the 95% confidence interval). The errors are mainly due to the whole of the
139 experiments (impregnation step, XRF analyses).

140 Transmission Electron Microscopy micrographs were obtained with a Philips CM200
141 microscope equipped with a LaB6 filament. The accelerating voltage was 200 kV.

142 Nitrogen physisorption analyses were performed on a Micromeritics Tristar apparatus. The
143 samples were first outgassed at 150 °C for 24 h under vacuum. Microporous volume ($cm^3.g_{ads}^{-1}$
144 or $cm^3.g_{SiO2}^{-1}$) was determined at $p/p^0 = 0.02$. Mesoporous volume was determined from the

desorption branch of the isotherm between $p/p^0 = 0.4$ and $p/p^0 = 0.9$. Pore size distributions were calculated by the BJH (Barrett-Joyner-Halenda) method on the desorption branch of the isotherm. From our numerous experiences on standard materials, the relative uncertainty of the adsorbed volume is estimated to 5 and 7% for results expressed in $cm^3.g_{ads}^{-1}$ and $cm^3.g_{SiO2}^{-1}$ STP respectively. For the pore diameter, it is close to 3%. The errors are mainly due to the impregnation step, laboratory weight scale and measurement apparatus.

2.4 SO_2 adsorption tests

The SO_2 adsorption and regeneration experiments were carried out on a home-made fully-automatized device in a fixed-bed configuration [1]. The SBA-CuO15_PCS or COK-CuO15_PCS (250-355 µm size) samples were deposited onto a fused silica frit (100 – 160 µm) in a tubular quartz reactor (internal diameter = 6 mm). The Gas Hourly Space Velocity (GHSV) was taken equal to 25000 h^{-1}. The SO_2 adsorption steps were performed under a 14 $NL.h^{-1}$ (SLPH – Standard Litre Per Hour) gas stream containing 250 ppmv of SO_2 and 10 vol.% of O_2 (balance N_2). SO_2 mole fraction at the reactor outflow was measured by an UV analyser. The adsorption step was systematically performed at 400 °C during 6000 s. The dynamic SO_2 chemisorption capacity ($C_{ads75\ ppmv}$ expressed in milligrams of adsorbed SO_2 per gram of CuO in the adsorbent material tested) was obtained through the integration of the SO_2 breakthrough curves until the SO_2 concentration at the outlet of the system reaches 75 ppmv. This integrated value is obtained as follows:

$$C_{ads75ppm} = \frac{F_v \int_{t_0}^{t_{75}} (C_0 - C)dt}{10^3\ V_m\ m_{CuO}}\ M_{SO2}$$

where F_v is the gas volumetric flow rate in $NL.h^{-1}$ (SLPH), C_0 and C are respectively the inlet (250 ppmv) and outlet SO_2 concentrations in ppmv, V_m is the molar volume of a gas (22.4 $L.mol^{-1}$ at 0 °C and 1 atm), m_{CuO} is the mass of CuO in the adsorbent within the fixed-bed in g, M_{SO2} is

the molecular mass of SO_2 (64 g.mol^{-1}), and t_0 and t_{75} (in h) are respectively the starting time and the time at which the SO_2 concentration reaches 75 ppmv.

The regeneration step was performed isothermally with the previous adsorption step, under a 14 NL.h^{-1} (SLPH) gaseous flow of 0.5 vol.% of H_2 (in N_2) gas mixture during 1200 s. The total SO_2 chemisorption capacity (i.e. the amount of SO_2 chemisorbed during the whole adsorption step expressed in mg_{SO2}/g_{CuO}) was obtained from the integration of the Temperature Programmed Desorption (TPD) curve from the start of the desorption step until less than 5 ppmv of SO_2 was detected on the analyser, as follows:

$$C_{adstotal} = \frac{F_v \int_{t_0}^{t_f} C\, dt}{10^3\, V_m\, m_{CuO}}\, M_{SO2}$$

where $C_{adstotal}$ is the total SO_2 chemisorption capacity of the adsorbent in mg_{SO2}/g_{CuO}, C is the outlet SO_2 concentration in ppmv, and t_0 and t_f (in h) are respectively the starting time and the time at which the SO_2 concentration reaches less than 5 ppmv.

The SBA-CuO15_PCS and COK-CuO15_PCS adsorbents were subjected to 15 adsorption-regeneration cycles.

The copper sulphation ratio (%) was determined as the ratio between SO_2-adsorbed species ($mol_{SO2}/g_{adsorbent}$) to the CuO content in the adsorbent (in $mol_{CuO}/g_{adsorbent}$).

The relative uncertainty of the adsorption capacities, was determined by means of the propagation of uncertainty method. They are estimated to 4 and 7% for total and dynamic SO_2 adsorption capacities respectively. The relative uncertainty of sulphation ratio is estimated close to 4%. Indeed, capacities are calculated from mass of CuO in the adsorbent, gas flow rate and concentration of SO_2 in gas phase, which are experimentally estimated and associated with measurement uncertainties. These uncertainties come from the use of mass flow meters, gas analysers, laboratory weight scale, and the impregnation step.

3. Results and discussion

Low angle X-ray diffraction patterns of SBA and COK samples, are shown in figure 1a.

(Figure 1)

Both samples exhibit three diffraction peaks in the low-angle region corresponding to the (100), (110) and (200) reflection planes of the hexagonal structure with P6mm symmetry (figure 1a). The diffraction profile of the COK sample is slightly shifted to smaller angles in comparison with the SBA sample and therefore, COK and SBA samples have lattice parameters of 10.7 and 10.3 nm, respectively. However, such short variation of lattice parameters could also be due to an artefact related to the sample holder used (glass plate, see experimental section).

Figure 1b shows diffraction patterns of SBA-CuO15 and COK-CuO15 samples. According to these patterns, no diffraction peaks of deleterious phases or CuO are observed which may indicate that copper species are in strong interaction with the supports, and therefore, homogeneously distributed on the supports. Moreover, the hexagonal structure of the support is preserved after the impregnation step (XRD patterns not reported) .

Figure 2 exhibits the nitrogen physisorption isotherms of SBA, COK, SBA-CuO15 and COK-CuO15 samples. The microporous and mesoporous volumes and pore diameter values are shown in Table 2. The adsorbed volumes were expressed in cm^3/g of adsorbent and cm^3/g of SiO_2.

(Figure 2)

(Table 2)

All samples exhibit type IV adsorption isotherms with H1-type hysteresis loop. Such isotherms correspond to mesoporous materials with well-ordered cylindrical pores, as defined by IUPAC [41].

The adsorption and desorption isotherms of SBA and COK samples have a different appearance. Despite a similar microporous volume, the COK sample shows a slightly higher mesoporous volume (0.60 vs 0.52 $cm^3 \cdot g^{-1}$ of SiO_2) than that of SBA-15. In addition, the COK sample shows a larger pore diameter (7.1 vs. 6.6 nm).

The isotherms of SBA-CuO15 and COK-CuO15 samples are quite different from those of the non-impregnated samples, in particular regarding the adsorbed volumes (y-axis). A decrease in microporous and mesoporous volume is observed which cannot be explained by the densification of the samples since the volumes expressed per gram of SiO_2 are also lower. In fact, SBA-CuO15 and COK-CuO15 samples show a decrease in mesoporous volume ($cm^3 \cdot g^{-1}$ of SiO_2) by 17% and 12%, respectively. Such a decrease might be due to the calcination at 500 °C to get the CuO adsorbents. However, the decrease in porous volumes (micro and meso) is more pronounced for the SBA-CuO15 sample. Therefore, the COK-CuO15 sample displays a higher mesoporosity (23%) than the SBA-CuO15 sample. In addition, the pore diameter decreases significantly for the SBA-CuO15 sample (6.2 nm instead of 6.6 nm for the SBA sample) compared to the COK-CuO15 sample, which presents similar pore diameter before and after the impregnation step (7.0 vs 7.1 nm for the COK sample).

When the samples are submitted to shaping in order to use them in the SO_x adsorption tests, the shaping has an impact on the porous volume of both samples. According to Table 2, the pelletized, crushed and sieved SBA-CuO15 and COK-CuO15 powders (SBA-CuO15_PCS and COK-CuO15_PCS, respectively) show a slightly decrease in micro and mesoporous volumes. On the other hand, the pore diameter does not change for both samples after shaping.

TEM and STEM micrographs of the SBA-CuO15 and COK-CuO15 samples are shown in figure 3.

(Figure 3)

TEM images (figures 3a, 3c) of the SBA-CuO15 and COK-CuO15 samples reveal the ordered hexagonal structure. STEM images (figures 3b, 3d) evidence the highly-dispersed active phase on the supports, in agreement with the XRD results. The images also reveal the difference particle shape of COK-12 compared to SBA-15. This is due to the typical tablet like morphology of COK-12 [21-23].

Figure 4 shows the SO_2 breakthrough curves for the first, fifth, tenth and fifteenth adsorption cycles for the SBA-CuO15_PCS and COK-CuO15_PCS adsorbents.

(Figure 4)

For the COK-CuO15_PCS adsorbent, the time to reach the SO_2 breakthrough decreases over the cycles. In the case of the SBA-CuO15_PCS adsorbent, this decrease is observed from the second cycle.

The evolution of the dynamic and total SO_2 adsorption capacity (see experimental section) expressed per $mg_{SO2}.g_{CuO}^{-1}$ and copper sulphation ratio along cycling experiments is presented in figure 5a and figure 5b, respectively.

(Figure 5)

The COK-CuO15_PCS adsorbent presents higher dynamic and total adsorption capacities than the SBA-CuO15_PCS adsorbent under 15 adsorption-regeneration cycles (figure 5a). After fifteen adsorption-regeneration cycles, the increase is close to 16% and 7%, respectively. For both SO_2 adsorption capacities, the difference between COK-CuO15_PCS and SBA-CuO15_PCS is close to the uncertainty of the measurement, but along all the cycles, these values are always higher for the COK-CuO15_PCS adsorbent. This behaviour difference may be related to the higher porosity of the COK-12 adsorbent, which would allow a better accessibility of SO_2 to the active sites. Another explanation could be the nature and the dispersion of the copper based active phase, which could be more different on the COK-12 support and slightly more efficient in SOx trapping. For both adsorbents, the total adsorption capacities are stable under 15 cycles. COK-CuO15_PCS and SBA-CuO15_PCS adsorbents exhibited a sulphation rate of 59% and 55%, respectively (figure 5b) which is close to the uncertainty of the measurement (4%).

When the total capacity is expressed in mg of SO_2 per gram of adsorbent, COK-CuO15_PCS and SBA-CuO15_PCS display total adsorption capacity of 76 and 70 $mg_{SO2}/g_{adsorbent}$, respectively, which is in accordance with previously published values also obtained with SBA-15 silica support [1, 4].

The results of structural, textural and microstructural characterization after the last adsorption and regeneration cycle are presented in figures 6, 7 and 8, respectively.

Wide angle X-ray diffraction patterns of the adsorbents after adsorption and regeneration multicycle experiments (COK-CuO15_PCS_AT and SBA-CuO15_PCS_AT samples) are shown in figure 6.

(Figure 6)

COK-CuO15_PCS_AT and SBA-CuO15_PCS_AT adsorbents exhibited two small diffraction peaks at 2Θ = 36.4º and 43.3° corresponding to the metallic copper (ICDD Nº 00-004-0836) and Cu_2O (ICDD Nº 00-005-0667) phases, respectively. The reductive regeneration step (0.5 vol.% of H_2 in N_2) of the sulphated adsorbents is responsible for the presence of Cuº [42]. While, the presence of the Cu_2O phase is due to the partial reduction of copper sulphate at 400 °C [43]. According to the literature, the sintering of Cu species can lead to a partial pore blocking of the support thus reducing its porous volume [4], while the presence of Cu^+ species is highly beneficial for the SO_x adsorption process [19, 42].

The nitrogen physisorption isotherms of COK-CuO15_PCS_AT and SBA-CuO15_PCS_AT adsorbents and their corresponding data are shown in figure 7 and Table 2, respectively.

(Figure 7)

After adsorption and regeneration multicycle experiments, the adsorbents showed a similar mesoporous volume decrease (close to 15-16%). Furthermore, the shape of the hysteresis loop of the SBA-CuO15_PCS adsorbent evolves from the type H1 to the type H5 after fifteen adsorption-regeneration cycles. According to IUPAC [41], the type H5 loop is related to a pore structure having opened and partial blocked mesopores. For the SBA-CuO15_PCS_AT adsorbent, the partial mesopore plugging is caused by the presence of copper-based nanoparticles, as highlighted by the diffraction patterns and TEM images (figure 8). The pore diameter decreases more sharply for the COK-CuO15_PCS sample after the cycling

311 experiments, however, its pore diameter still remained higher than for the SBA-CuO15_PCS
312 sample (6.4 vs 5.9 nm).
313 TEM micrographs of the aged adsorbents (SBA-CuO15_PCS_AT and COK-CuO15_PCS_AT
314 samples) are shown in figure 8a and figure 8b, respectively.

315

316 **(Figure 8)**

317

318 These results highlight the sintering of copper species in both SBA-15 and COK-12 supports. It
319 is also observed that some copper-based particles are larger than the pores size of the supports
320 and therefore are on their surface. Despite the sintering phenomenon, SBA-CuO15_PCS and
321 COK-CuO15_PCS adsorbents preserve their adsorption capacity over the fifteen adsorption-
322 regeneration cycles.

323

324 **4. Conclusion**

325 The study of the effect of the support on the structural, textural and SO_x adsorption properties of
326 CuO/SBA-15 and CuO/COK-12 adsorbents provides interesting results. The XRD analyses
327 confirm the hexagonal structure of the SBA-15 and COK-12 supports. The impregnation and
328 shaping processes have an impact on textural properties. SBA-CuO15_PCS and COK-
329 CuO15_PCS adsorbents presented a total loss of 38% and 33% of the mesoporous volume,
330 respectively. Moreover, pore diameter is decreased significantly for the SBA-CuO sample after
331 the impregnation process. Highly-dispersed active phase-based SBA-CuO15_PCS and COK-
332 CuO15_PCS adsorbents have been tested in SO_2 adsorption and regeneration experiments. The
333 COK-CuO15_PCS adsorbent displays higher dynamic adsorption capacities than SBA-
334 CuO15_PCS under 15 adsorption-regeneration cycles. Such a result could be explained by a

335 better accessibility of SO_2 to the active sites of the COK-CuO15_PCS adsorbent, due to its larger
336 porosity and shorter mesopores due to a more favourable particle morphology. Despite the
337 sintering phenomenon, the SBA-CuO15_PCS and COK-CuO15_PCS adsorbents preserve their
338 SO_2 adsorption capacity over the cycling experiments. Therefore, COK-12 support for the CuO
339 active phase appears to be quite promising as SO_2 adsorbents also taking into account the
340 simplicity of the preparation method and its cost.

341

342 **5. Acknowledgements**

343 The authors want to gratefully acknowledge the French Agency for Environment and Energy
344 Management (ADEME) for its financial support and Laure Michelin for the XRD analyses and
345 Loic Vidal for the TEM and STEM analyses, which were performed on the technical platforms
346 of IS2M. JAM acknowledges the Flemish Government for long-term structural funding
347 (Methusalem).

348

349

350

351 **6. Formatting of funding sources**

352 This work was supported by the French Agency for Environment and Energy Management
353 (ADEME) through its funding program CORTEA (Project AdSOx –contract #1781C0019).

354

355 **7. References**

356 [1] M. Berger, S. Dorge, H. Nouali, D. Habermacher, E. Fiani, M. Vierling, M. Molière, J.F.
357 Brilhac, J. Patarin, Role of the process conditions on the sulphation and stability of a CuO/SBA-

15 type SOx adsorbent in cycling operations, Chem. Eng. J. 350 (2018) 729-738. https://doi.org/10.1016/j.cej.2018.05.170.

[2] R.C. Flagan, J.H. Seinfeld, Fundamentals of air pollution engineering, Englewood Cliffs, New Jersey, 1988.

[3] G.E. Likens, F.H. Bormann, Acid Rain: A serious regional environmental problem, Science 184 (1974) 1176-1179. https://doi.org/10.1126/science.184.4142.1176.

[4] M. Berger, H. Nouali, S. Dorge, D. Habermacher, E. Fiani, M. Vierling, M. Molière, C. Schönnenbeck, J.F. Brilhac, J. Patarin, Long-term activity of a CuO/SBA-15 type SOx adsorbent: Impact of the regeneration step, Chem. Eng. J. 347 (2018) 202-213. https://doi.org/10.1016/j.cej.2018.04.066.

[5] P. Gaudin, L. Michelin, L. Josien, H. Nouali, S. Dorge, J.F. Brilhac, E. Fiani, M. Vierling, M. Molière, J. Patarin, Highly dispersed copper species supported on SBA-15 mesoporous materials for SOx removal: Influence of the CuO loading and of the support, Fuel Process. Technol. 148 (2016) 1-11. https://doi.org/10.1016/j.fuproc.2016.02.025.

[6] G. Buelna, Y.S. Lin, Characteristics and desulfurization-regeneration properties of sol–gel-derived copper oxide on alumina sorbents, Sep. Purif. Technol. 39 (2004) 167-179. https://doi.org/10.1016/S1383-5866(03)00183-7.

[7] H.H. Tseng, M.Y. Wey, Study of SO_2 adsorption and thermal regeneration over activated carbon-supported copper oxide catalysts, Carbon 42 (2004) 2269-2278. https://doi.org/10.1016/j.carbon.2004.05.004.

[8] P. Gaudin, S. Dorge, H. Nouali, D. Kehrli, L. Michelin, L. Josien, P. Fioux, L. Vidal, M. Soulard, M. Vierling, M. Molière, J.F. Brilhac, J. Patarin, Synthesis of Cu-Ce/KIT-6 materials

for SOx removal, Appl. Catal. A. 504 (2015) 110-118. https://doi.org/10.1016/j.apcata.2014.11.024.

[9] G. Centi, N. Passarini, S. Perathoner, A. Riva, Combined DeSOx/DeNOx Reactions on a copper on alumina sorbent-catalyst.1. Mechanism of SO_2 oxidation-adsorption, Ind. Eng. Chem. Res. 31(1992) 1947-1955. https://doi.org/10.1021/ie00008a016.

[10] S.S. Pollack, W.P. Chisholm, R.T. Obermyer, S.W. Hedges, M. Ramanathan, P.A. Montana, Properties of copper/alumina sorbents used for the removal of sulfur dioxide, Ind. Eng. Chem. Res. 27 (1988) 2276–2282. https://doi.org/10.1021/ie00084a013.

[11] G. Centi, S. Perathoner, Role of the Size and Texture Properties of Copper-on-Alumina Pellets during the simultaneous removal of SO_2 and NOx from flue gas, Ind. Eng. Chem. Res. 36 (1997) 2945–2953. https://doi.org/10.1021/ie9604886.

[12] K.S. Yoo, S.D. Kim, S.B. Park, Sulfation of AI_2O_3 in flue gas desulfurization by CuO/γ-AI_2O_3 sorbent, Ind. Eng. Chem. Res. 33 (1994) 1786–1791. https://doi.org/10.1021/ie00031a018.

[13] Y. Yuono, D. Bahrin, H. Susanto, Preparation and Characterization of CuO/γ-Al_2O_3 for Adsorption of SO_2 in flue gas Mod. Appl. Sci. 9 (2015) 107–113. http://dx.doi.org/10.5539/mas.v9n7p107.

[14] D. Bahrin, Subagjo, H. Susanto, Effect of tegeneration temperature on particle characteristics and extent of regeneration of saturated SO_2-Adsorption of CuO/γ-Al_2O_3 adsorbent, Procedia Chem. 16 (2015) 723–727. https://doi.org/10.1016/j.proche.2015.12.020.

[15] H.H. Tseng, M.Y. Wey, C.H. Fu, Carbon materials as catalyst supports for SO_2 oxidation: Catalytic activity of CuO–AC, Carbon 41 (2003) 139–149. https://doi.org/10.1016/S0008-6223(02)00264-6.

[16] V. Gaur, A. Sharma, N. Verma, Removal of SO_2 by activated carbon fibre impregnated with transition metals, Can. J. Chem. Eng. 85 (2007) 188–198. https://doi.org/10.1002/cjce.5450850207.

[17] H. Yi, Y. Zuo, H. Liu, X. Tang, S. Zhao, B. Zhang, Z. Wang, F. Gao, Study on coadsorption of SO_2, NO, and CO_2 over copper-supported activated carbon sorbent in different operating conditions, Environ. Prog. Sustain. Energy 34 (2015) 1044–1049. https://doi.org/10.1002/ep.12098.

[18] P. Gaudin, S. Dorge, H. Nouali, J. Patarin, J.F. Brilhac, E. Fiani, M. Vierling, M. Molière, Synthesis of CuO/SBA-15 adsorbents for SOx removal applications, using different impregnation methods, C. R. Chim. 18 (2015) 1013-1029. https://doi.org/10.1016/j.crci.2015.07.002.

[19] P. Gaudin, P. Fioux, S. Dorge, H. Nouali, M. Vierling, E. Fiani, M. Molière. J.F. Brilhac, J. Patarin, Formation and role of Cu^+ species on highly dispersed CuO/SBA-15 mesoporous materials for SOx removal: An XPS study, Fuel Process. Technol. 153 (2016) 129-136. https://doi.org/10.1016/j.fuproc.2016.07.015.

[20] N. Rahmat, A.Z. Abdullah, A.R. Mohamed, A Review: Mesoporous Santa Barbara amorphous-15, types, synthesis and its applications towards biorefinery production, Am. J. Appl. Sci. 7 (2010) 1579-1586. https://doi.org/10.3844/ajassp.2010.1579.1586.

[21] J. Jammaer, A. Aerts, J. D'Haen, J.W. Seo, J.A. Martens, Convenient synthesis of ordered mesoporous silica at room temperature and quasi-neutral pH, J. Mater. Chem. 19 (2009) 8290–8293. https://doi.org/10.1039/B915273C.

[22] J.A. Martens, J. Jammaer, S. Bajpe, A. Aerts, Y. Lorgouilloux, C.E.A. Kirschhock, Simple synthesis recipes of porous materials, Micropor. Mesopor. Mater. 140 (2011) 2–8. https://doi.org/10.1016/j.micromeso.2010.09.018.

[23] J. Jammaer, T.S. van Erp, A. Aerts, C.E.A. Kirschhock, J.A. Martens, Continuous synthesis process of hexagonal nanoplates of P6m ordered mesoporous silica, J. Am. Chem. Soc. 133 (2011) 13737-13745. https://doi.org/10.1021/ja205627t.

[24] M. Vialpando, A. Aerts, J. Persoons, J. Martens, G. Van Den Mooter, Evaluation of ordered mesoporous silica as a carrier for poorly soluble drugs: Influence of pressure on the structure and drug release, J. Pharm. Sci. 100 (2011) 3411-3420. https://doi.org/10.1002/jps.22535.

[25] M.G. Colmenares, U. Simon, M. Yildiz, S. Arndt, R. Schomaecker, A. Thomas, F. Rosowski, A. Gurlo, O. Goerke, Oxidative coupling of methane on the Na_2WO_4-Mn_xO_y catalyst: COK-12 as an inexpensive alternative to SBA-15, Catal. Commun. 85 (2016) 75–78. https://doi.org/10.1016/j.catcom.2016.06.025.

[26] M.G. Colmenares, U. Simon, O. Cruz, A. Thomas, O. Goerke, A. Gurlo, Batch and continuous synthesis upscaling of powder and monolithic ordered mesoporous silica COK-12, Micropor. Mesopor. Mater. 256 (2018) 102-110. https://doi.org/10.1016/j.micromeso.2017.08.002.

[27] M.G. Colmenares, U. Simon, F. Schmidt, S. Dey, J. Schmidt, A. Thomas, A. Gurlo, Tailoring of ordered mesoporous silica COK-12: Room temperature synthesis of mesocellular foam and multilamellar vesicles, Micropor. Mesopor. Mater. 267 (2018) 142-149. https://doi.org/10.1016/j.micromeso.2018.03.015.

[28] L.M. Henning, D.D. Cubas, M.G. Colmenares, J. Schmidt, M.F. Bekheet, B.R. Pauw, A. Gurlo, U. Simon, High specific surface area ordered mesoporous silica COK-12 with tailored

pore size, Micropor. Mesopor. Mater. 280 (2019) 133–143. https://doi.org/10.1016/j.micromeso.2019.01.050.

[29] M. Varkolu, V. Velpula, S. Ganji, D.R. Burri, S.R.R. Kamaraju, Ni nanoparticles supported on mesoporous silica (2D, 3D) architectures: Highly efficient catalysts for the hydrocyclization of biomass-derived levulinic acid, RSC Adv. 5 (2015) 57201-57210. https://doi.org/10.1039/C5RA10857H.

[30] S.P. Sree, J. Dendooven, J. Jammaer, K. Masschaele, D. Deduytsche, J. D'Haen, C.E.A. Kirschhock, J.A. Martens, C. Detavernier, Anisotropic atomic layer deposition profiles of TiO_2 in hierarchical silica material with multiple porosity, Chem. Mater. 24 (2012) 2775-2780. https://doi.org/10.1021/cm301205p.

[31] W. Janssens, E.V. Makshina, P. Vanelderen, F. De Clippel, K. Houthoofd, S. Kerkhofs, J.A. Martens, P.A. Jacobs, B. F. Sels, Ternary Ag/MgO-SiO_2 catalysts for the conversion of ethanol into butadiene, ChemSusChem 8 (2015) 994-1008. https://doi.org/10.1002/cssc.201402894.

[32] L. Wang, M. Zhang, M. Zhang, G. Sha, C. Liang, Hydrodeoxygenation of dibenzofuran over mesoporous silica COK-12 supported palladium catalysts, Energy Fuels 27 (2013) 2209-2217. https://doi.org/10.1021/ef302166q.

[33] R. Pochamoni, A. Narani, M. Varkolu, M.D. Gudimella, S.S.P. Potharaju, D.R. Burri, S.R.R. Kamaraju, Studies on ethylbenzene dehydrogenation with CO_2 as soft oxidant over Co_3O_4/COK-12 catalysts, J.of Chem. Sci. 127 (2015) 701–709. https://doi.org/10.1007/s12039-015-0826-x.

[34] R. Pochamoni, A. Narani, V.R.B. Gurram, M.D. Gudimella, P.S.S.P. Potharaju, D.R. Burri, K S.R. Rao, Molybdenum oxide supported on COK-12: A novel catalyst for oxidative dehydrogenation of ethylbenzene using CO_2, Ind. J. of Chem. 53A (2014) 493-498. http://nopr.niscair.res.in/bitstream/123456789/28464/2/IJCA%2053A%284-5%29%20493-498.pdf

[35] L.H. Wee, M. Meledina, S. Turner, K. Custers, S. Kerkhofs, G. van Tendeloo, J.A. Martens, Hematite iron oxide nanorod patterning inside COK-12 mesochannels as an efficient visible light photocatalyst, J. Mater. Chem. A. 3 (2015) 19884-19891. https://doi.org/10.1039/C5TA05075H.

[36] L.H. Wee, M. Meledina, S. Turner, K. Custers, S. Kerkhofs, S.P. Sree, E. Gobechiya, C.E.A. Kirschhock, G. Van Tendeloo, J.A. Martens, Anatase TiO_2 nanoparticle coating on porous COK-12 platelets as highly active and reusable photocatalysts, RSC Adv. 6 (2016) 46678-46685. https://doi.org/10.1039/C6RA06141A.

[37] M. Tasbihi, F. Fresno, U. Simon, I.J. Villar-García, V. Pérez-Dieste, C. Escudero, V.A. de la Peña O'Shea, On the selectivity of CO_2 photoreduction towards CH_4 using Pt/TiO_2 catalysts supported on mesoporous silica, Appl. Catal. B Environ. 239 (2018) 68-76. https://doi.org/10.1016/j.apcatb.2018.08.003.

[38] A.L. Khan, S.P. Sree, J.A. Martens, M.T. Raza, I.F.J. Vankelecom, Mixed matrix membranes comprising of matrimid and mesoporous COK-12: Preparation and gas separation properties, J. Membr. Sci. 495 (2015) 471-478. https://doi.org/10.1016/j.memsci.2015.08.008.

[39] A.J. Bagnall, M.S. Vega, J. Martinelli, K. Djanashvili, F. Cucinotta, Mesoscopic FRET antenna materials by self-assembling iridium(III) complexes and BODIPY Dyes, Chem. Eur. J. 24 (2018) 11992-11999. https://doi.org/10.1002/chem.201802745.

[40] M. Vialpando, F. Backhuijs, J.A. Martens, G. Van den Mooter, Risk assessment of premature drug release during wet granulation of ordered mesoporous silica loaded with poorly soluble compounds itraconazole, fenofibrate, naproxen, and ibuprofen, Eur. J. Pharm. Biopharm. 81 (2012) 190-198. https://doi.org/10.1016/j.ejpb.2012.01.012.

[41] M. Thommes, K. Kaneko, A.V. Neimark, J.P. Olivier, F. Rodriguez-Reinoso, J. Rouquerol, K.S.W. Sing, Physisorption of gases, with special reference to the evaluation of surface area and

pore size distribution (IUPAC Technical Report), Pure Appl. Chem. 87 (2015) 1051–1069. https://doi.org/10.1515/pac-2014-1117.

[42] M. Berger, P. Fioux, S. Dorge, H. Nouali, D. Habermacher, E. Fiani, M. Vierling, M. Moliere, J.F. Brilhac, J. Patarin, Structure-performance relationship in CuO/SBA-15-type SOx adsorbent: evolution of copper-based species under different regenerative treatments, Catal. Sci. Technol. 7 (2017) 4115-4128. https://doi.org/10.1039/C7CY01010A.

[43] N. Jacinto, S.N. Sinha, M. Nagamori, H.Y. Sohn, An equilibrium study of the hydrogen reduction of copper sulfates, Metall. Trans. B 14 (1983) 136-139. https://doi.org/10.1007/BF02654063.

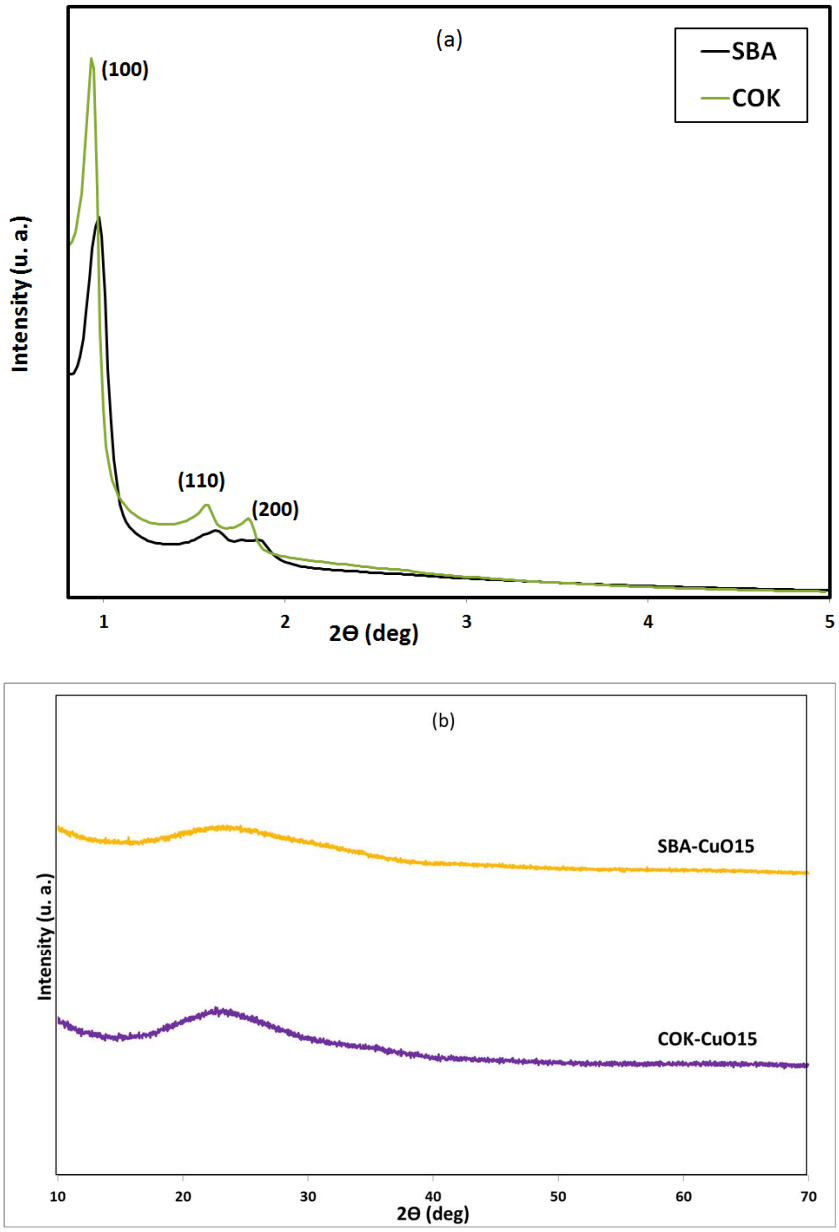

Figure 1: (a) Low angle XRD patterns of SBA and COK samples and (b) wide-angle XRD patterns of SBA-CuO15 and COK-CuO15 samples.

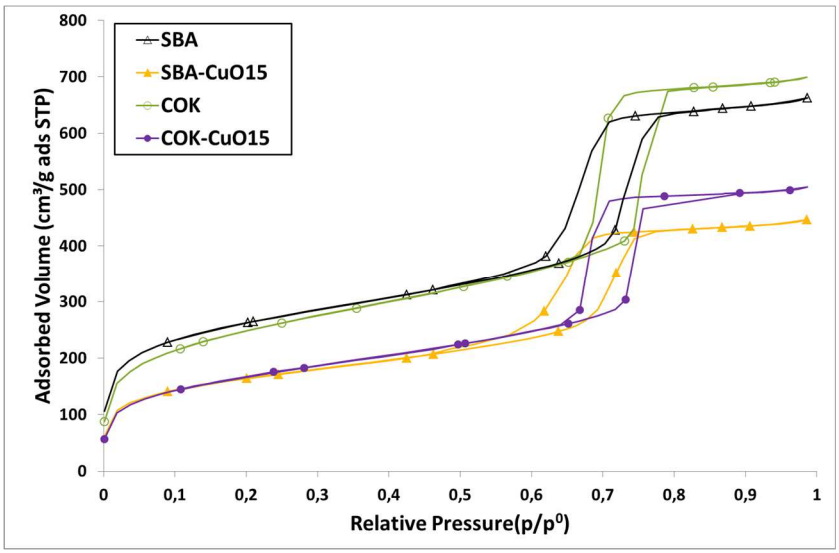

Figure 2: Nitrogen physisorption isotherms at – 196 °C of SBA, COK, SBA-CuO15 and COK-CuO15 samples.

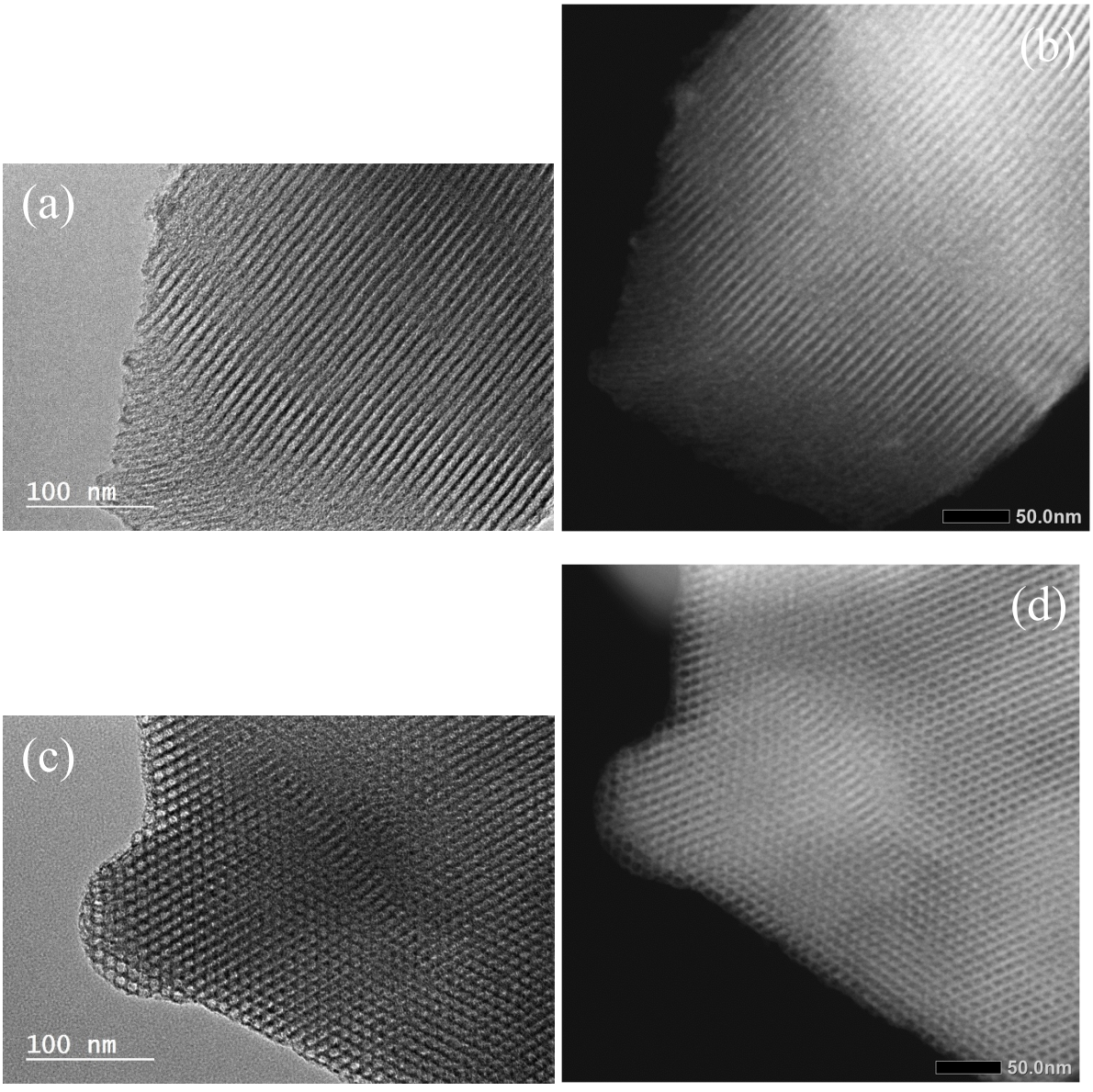

Figure 3: TEM (a, c) and STEM (b, d) micrographs of SBA-CuO15 (a,b) and COK-CuO15 (c,d) samples.

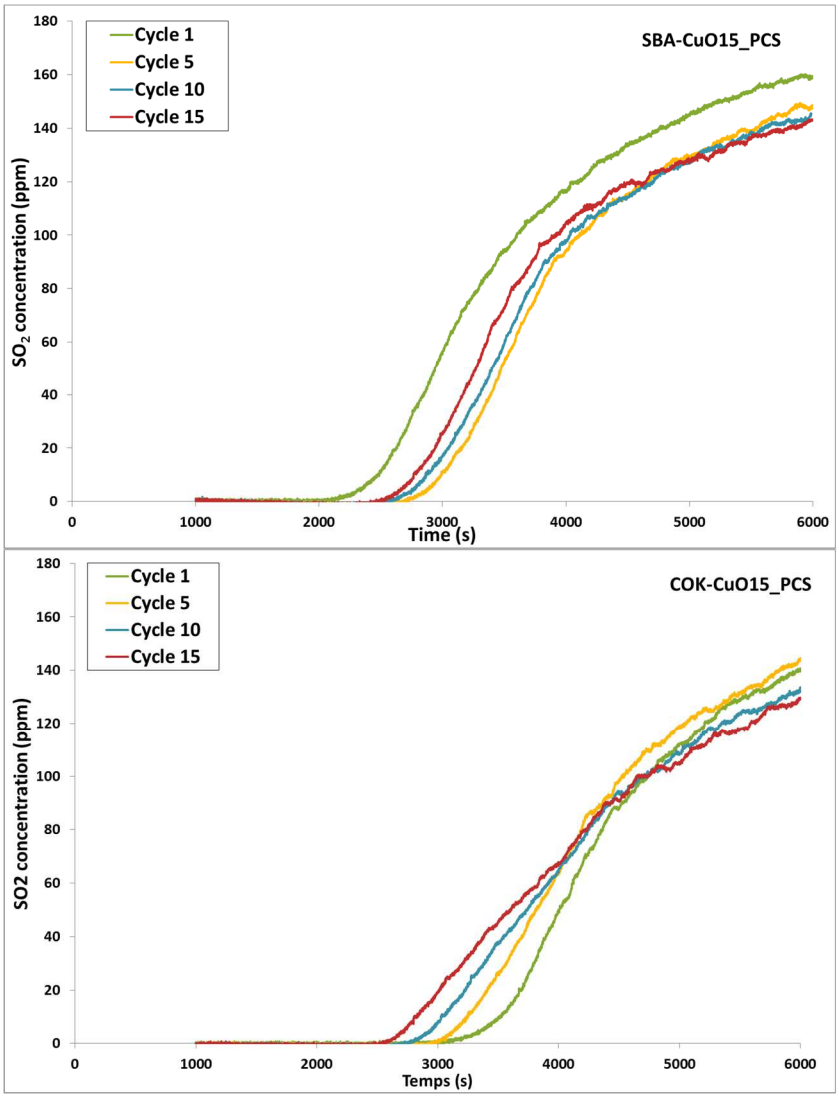

Figure 4: SO_2 breakthrough curves of SBA-CuO15_PCS and COK-CuO15_PCS samples, after first, fifth, tenth and fifteenth adsorption and regeneration cycles.

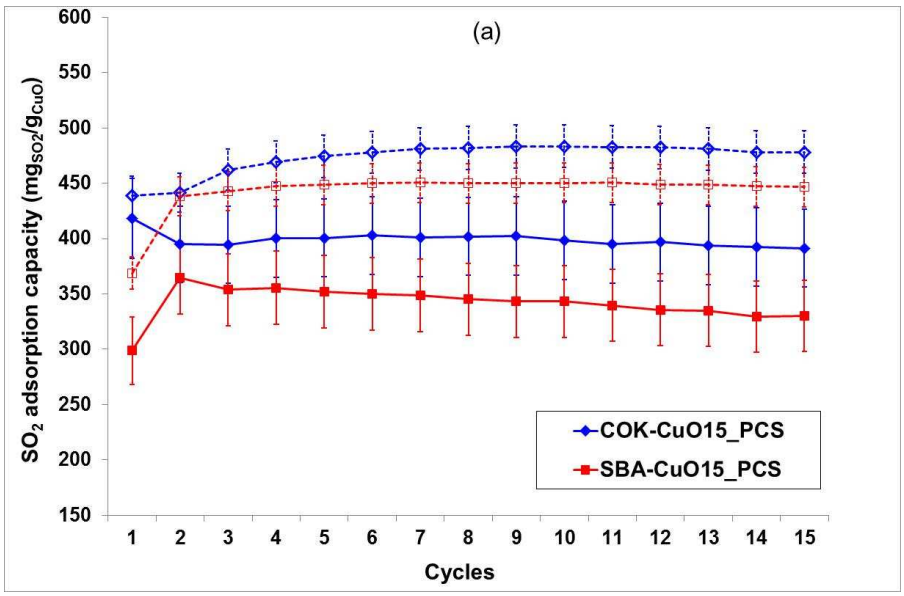

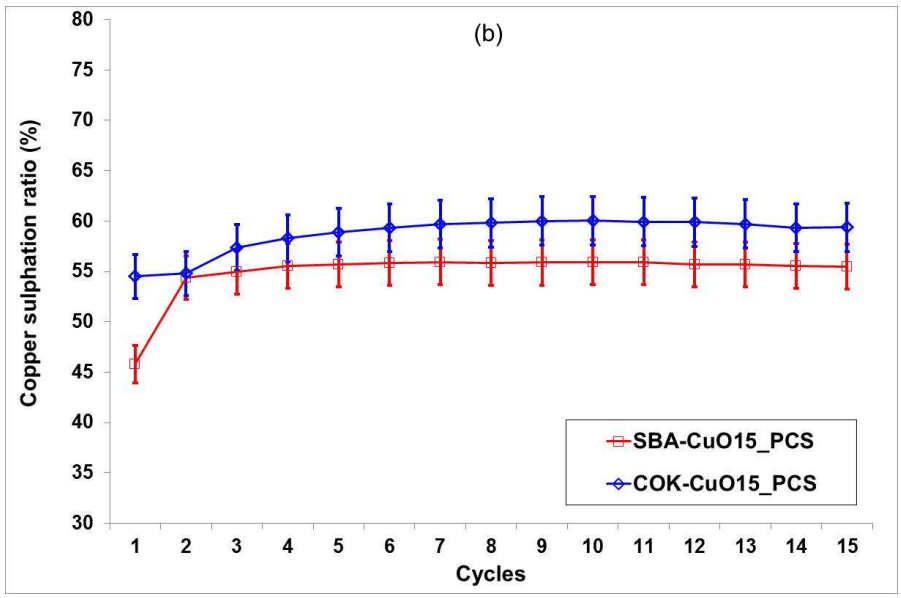

Figure 5: Evolution of the dynamic (filled symbol) and total (empty symbol) SO_2 adsorption capacities (a) and copper sulphation ratio (b) during 15 adsorption and regeneration cycles of SBA-CuO15_PCS and COK-CuO15_PCS samples.

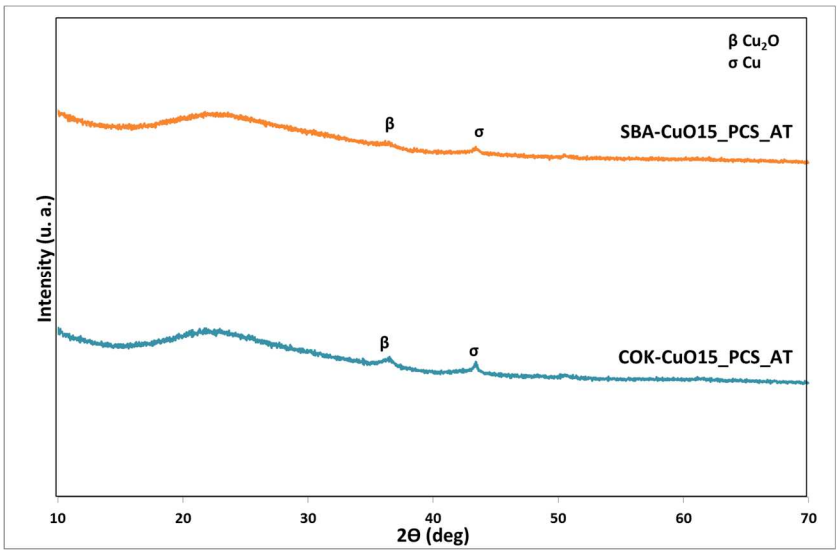

Figure 6: Wide-angle XRD patterns of SBA-CuO15_PCS_AT and COK-CuO15_PCS_AT samples.

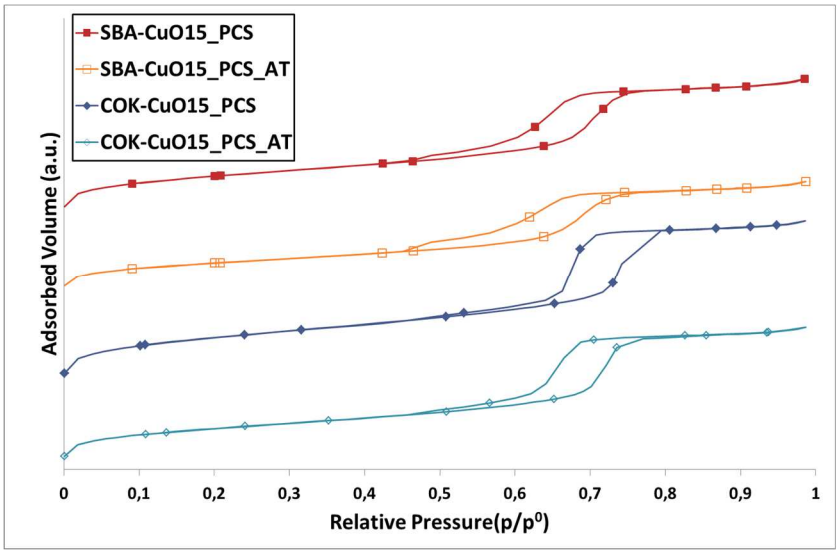

Figure 7: Nitrogen physisorption isotherms at – 196 °C of SBA-CuO15_PCS and COK-CuO15_PCS samples before and after (AT) adsorption and regeneration multicycle experiments. For a better visibility, the isotherms are shifted along the Y-axis.

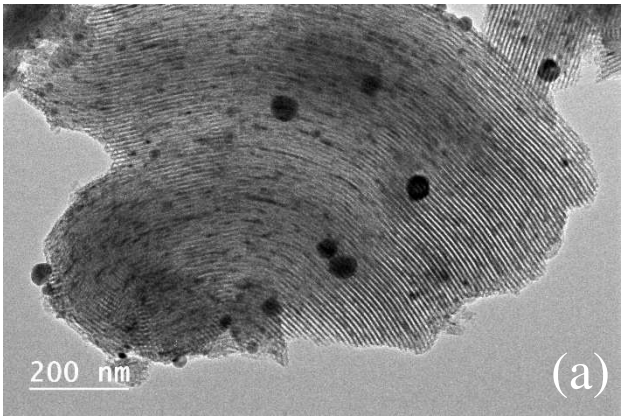

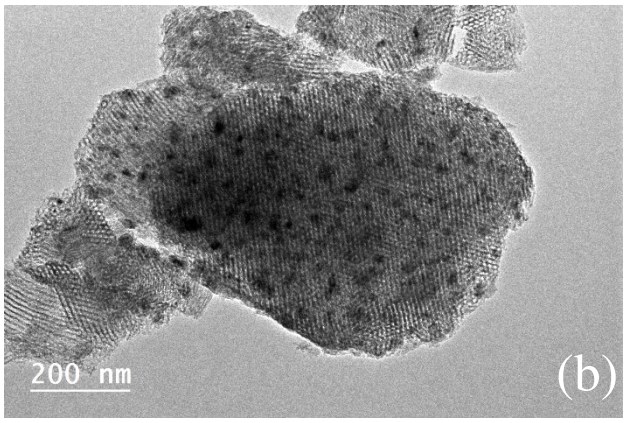

Figure 8: TEM micrographs of SBA-CuO15_PCS_AT (a) and COK-CuO15_PCS_AT (b) samples.

List of tables:

Table 1 – Nomenclature of prepared samples.

Samples	Nomenclature
SBA-15 powder	SBA
COK-12 powder	COK
SBA-15 powder impregnated with 15 wt.% of copper oxide and calcined at 500 ºC	SBA-CuO15
Pelletized, Crushed and Sieved (250-355 µm) SBA-CuO15 powder	SBA-CuO15_PCS
COK-12 powder impregnated with 15 wt.% of copper oxide and calcined at 500 ºC	COK-CuO15
Pelletized, Crushed and Sieved (250-355 µm) COK-CuO15 powder	COK-CuO15_PCS

Table 2 – Textural properties of SBA and COK samples and of their CuO-containing derivatives before and after (AT) the last adsorption and regeneration test. The CuO content (wt.%) in the impregnated samples is also shown.

Sample	% of CuO (wt.%)[a]	Porous volume[b]				Pore diameter (nm)[e]
		Microporous[c]		Mesoporous[d]		
		(cm^3/g_{ads})	(cm^3/g_{SiO2})	(cm^3/g_{ads})	(cm^3/g_{SiO2})	
SBA		0.27 ± 0.01	0.27 ± 0.02	0.52 ± 0.03	0.52 ± 0.04	6.6 ± 0.2
SBA-CuO15	15.6 ± 0.3	0.17 ± 0.01	0.20 ± 0.01	0.37 ± 0.02	0.43 ± 0.03	6.2 ± 0.2
SBA-CuO15_PCS	---	0.13 ± 0.01	0.15 ± 0.01	0.32 ± 0.02	0.38 ± 0.03	6.0 ± 0.2
SBA-CuO15_PCS_AT	---	0.10 ± 0.01	0.12 ± 0.01	0.27 ± 0.01	0.32 ± 0.02	5.9 ± 0.2
COK		0.24 ± 0.01	0.24 ± 0.02	0.60 ± 0.03	0.60 ± 0.04	7.1 ± 0.2
COK-CuO15	15.8 ± 0.3	0.16 ± 0.01	0.19 ± 0.01	0.45 ± 0.02	0.53 ± 0.04	7.0 ± 0.2
COK-CuO15_PCS	---	0.14 ± 0.01	0.16 ± 0.01	0.40 ± 0.02	0.47 ± 0.03	6.9 ± 0.2
COK-CuO15_PCS_AT	---	0.10 ± 0.01	0.12 ± 0.01	0.34 ± 0.02	0.40 ± 0.03	6.4 ± 0.2

[a] Determined by XRF analysis. The two values are similar; the relative uncertainty is estimated to 2%.
[b] The relative uncertainty is equal to 5 and 7% for porous volume expressed in $cm^3/g_{adsorbent}$ and cm^3/g_{SiO2} respectively
[c] Determined from the adsorbed volume at p/p^0=0.02.
[d] Determined from the desorption branch of the isotherm between p/p^0= 0.4 and p/p^0= 0.9.
[e] Determined from raw data using the BJH method on the desorption branch. The relative uncertainty is equal to 3%.

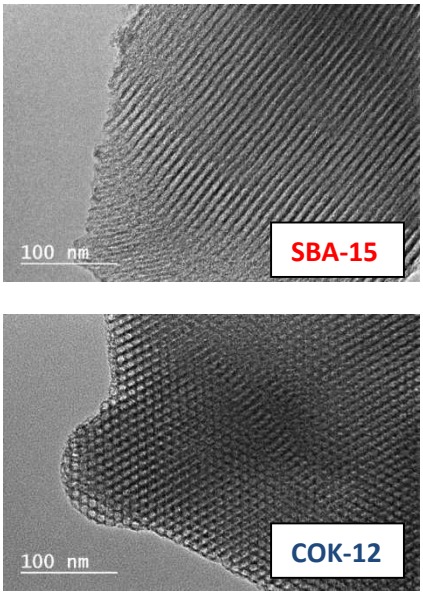

Impregnation by 15 wt.% of CuO

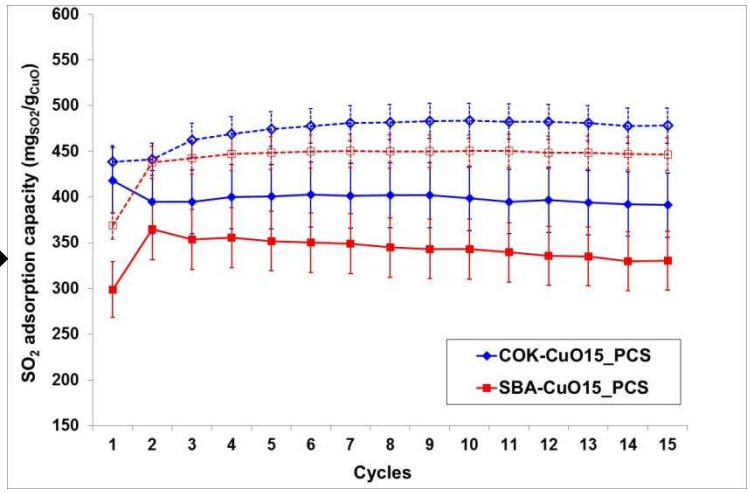

SO_2 adsorption capacity: COK-CuO15 > SBA-CuO15